Bioorganic Chemistry 57 (2014) 206–212

Contents lists available at ScienceDirect

Bioorganic Chemistry

journal homepage: www.elsevier.com/locate/bioorg

Reflections on the catalytic power of a TIM-barrel

John P. Richard *, Xiang Zhai, M. Merced Malabanan

Department of Chemistry, University at Buffalo, SUNY, Buffalo, NY 14260, United States

ARTICLE INFO

Article history:
Available online 11 July 2014

Keywords:
Enzyme
Catalysis
Proton transfer
TIM-barrel
Protein structure
Enolate

ABSTRACT

The TIM-barrel fold is described and its propagation throughout the enzyme universe noted. The functions of the individual front loops of the eponymous TIM-barrel of triosephosphate isomerase are presented in a discussion of: (a) electrophilic catalysis, by amino acid side chains from loops 1 and 4, of abstraction of an α-carbonyl hydrogen from substrate dihydroxyacetone phosphate (DHAP) or D-glyceraldehyde 3-phosphate (DGAP). (b) The engineering of loop 3 to give the monomeric variant monoTIM and the structure and catalytic properties of this monomer. (c) The interaction between loops 6, 7 and 8 and the phosphodianion of DHAP or DGAP. (d) The mechanism by which a ligand-gated conformational change, dominated by motion of loops 6 and 7, activates TIM for catalysis of deprotonation of DHAP or DGAP. (e) The conformational plasticity of TIM, and the utilization of substrate binding energy to "mold" the distorted active site loops of TIM mutants into catalytically active enzymes. The features of the TIM-barrel fold that favor effective protein catalysis are discussed.

1. Introduction

Protein structure determines function in obtaining large enzymatic rate enhancements [1–6]. An interesting and difficult problem is to define the mechanism by which specific features of folded α-helices, β-strands and flexible loops contribute to these rate enhancements. The classical TIM-barrel fold $(\beta\alpha)_8$ consists of eight repeating (βα) units arranged so that eight parallel β-strands form a central protein core that is covered by α-helices on the outside. The TIM-barrel is reportedly the most common protein fold in the Protein Data Bank, and at one time accounted for about 10% of all proteins with known three-dimensional structures [7–9]. The properties of this protein fold [8,10], and the divergent evolution of the progenitor TIM-barrel into proteins that display a vast array of enzymatic activities, have been discussed in many excellent reviews [8–14]. This essay will consider the specific features of the TIM-barrel, which favor efficient catalysis by the eponymous enzyme triosephosphate isomerase (TIM); and, the general features of this protein fold, which favored propagation of the TIM-barrel throughout the enzyme universe.

The secondary structural elements of the TIM-barrel are numbered sequentially from the N-terminus as β1–β8 and α1–α8. These strands and helices are connected by a total of sixteen loops, which are referred to as βα loops (front loops), such that the βα loop 1 follows after strand β1; and, αβ loops (back loops), such that αβ loop 1 follows after helix α1. The active sites of TIM-barrel enzymes lie at the C-terminal ends of the β-strands, which are localized at the "catalytic" end of the barrel. They are often constructed by the folding of the eight βα front loops into a structured *cage* for the substrate, whose formation is driven by the development of stabilizing interactions between the substrate and the catalytic front loops [15] The eight back loops lie at the end of the barrel distant from the front loops, and play an important role in stabilizing this protein fold [8,11]. The TIM-barrel provides a robust framework to support an incredible variety of front loop structures, which are used in construction of the active sites for enzymes found in 21 homologous superfamilies and 76 different sequence families [10].

2. Triosephosphate isomerase

[1]The TIM-barrel fold was first characterized for the crystal structure for triosephosphate isomerase (TIM), which catalyzes isomerization of D-glyceraldehyde 3-phosphate (GAP) to dihydroxyacetone phosphate (DHAP, Scheme 1), through a pair of enediolate reaction intermediates [20]. Enzyme-catalyzed isomerization proceeds with proton transfer between carbons 1 and 2, mediated by the carboxylate side chain of Glu165 [16,17], and between oxygen 1 and 2, mediated by the imidazole side chain of His95 [18,19].

* Corresponding author. Fax: +1 (716) 645 6963.
E-mail address: jrichard@buffalo.edu (J.P. Richard).

[1] We note the following small differences in the numbering of the amino acid residues at TIM from the different sources: (*c*TIM or *y*TIM and *Tbb*TIM): Lys 12 and 13, Glu165 and 167, Pro166 and 168, Ile170 and 172, Leu230 and 232.

http://dx.doi.org/10.1016/j.bioorg.2014.07.001
0045-2068/

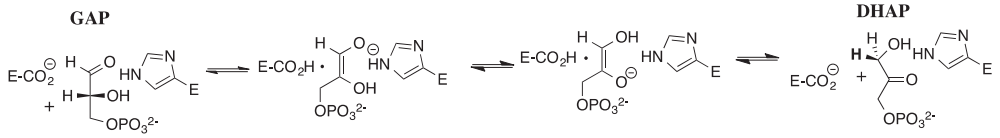

Scheme 1. An abbreviated mechanism for TIM-catalyzed isomerization of D-glyceraldehyde 3-phosphate (GAP) to dihydroxyacetone phosphate (DHAP). Proton transfer reactions at carbon and oxygen are carried out, respectively, by the carboxylate side chain of Glu165 [16,17] and the imidazole side chain of His95 [18,19].

The side chains of Asn10 and Lys12 are positioned to provide stabilization of the developing negative charge at either O-1 or O-2 of enediolate phosphate reaction intermediates [21,22]. The mechanism of action of TIM has been investigated by kinetic and isotope labeling studies [23–27], the specific role of the active site side chains has been probed by site-directed mutagenesis [20,28–31], and the role of an extended ligand-gated conformational change has been examined in solid state [32,33] and solution NMR studies [34,35] and by temperature jump relaxation fluorescence spectroscopy [36].

This essay will focus on the function of the front loops of the TIM-barrel in catalysis of isomerization of DGAP, and will conclude by drawing generalizations from these studies about the advantages of the TIM-barrel that favor its evolution into proteins that catalyze a broad range of reactions. Fig. 1A and B shows representations of chicken muscle TIM (*c*TIM) from the top and the side of the TIM-barrel, respectively, which highlight the β1–β8 front loops from a single enzyme subunit, and the β1–β8 loop 3′ from the neighboring subunit. The loops are grouped by colors and the codes are given in the figure legend.

2.1. Loops 1 and 4

Efficient catalysis by TIM requires that the enzyme provide a similar lowering of the activation barriers to proton transfer at carbon-1 of DHAP and carbon-2 of GAP, in order to avoid one of these steps become strongly rate-determining for turnover. Consequently, the basic side chain of Glu165 shows a similar high reactivity toward deprotonation of C-1 and C-2 of DHAP and DGAP, respectively. It is not widely appreciated that the reactivity of this side chain depends upon both its intrinsic basicity and upon the assistance to carbon deprotonation from electrophilic catalysis at the carbonyl oxygen of DHAP or DGAP. This sets TIM an additional challenge of providing strong stabilization of transition state negative charge that develops at O-1, when the substrate is DGAP, and at O-2 when the substrate is DHAP; while, at the same time promoting fast intramolecular transfer of hydrogen between O-1 and O-2 in the overall isomerization reaction (Scheme 1).

Three acidic side chains are positioned to stabilize negative charge at the two enediolate intermediates (Fig. 2A): the amide side chain from Asn10, the alkylammonium side chain from Lys12 (loop one, residues 12–17 for *c*TIM) [22,41,42], and the imidazole side chain of His95 (loop 4, residues 94–105 for *c*TIM) [18,19,43]. The imidazole side chain lies equidistant from O-1 and O-2 at the complexes to the intermediate analog PGH (Fig. 2B) for TIM from *L. mexicana* [38]. This implies a role for the side chain in mediating proton transfer between O-1 and O-2 (Scheme 1). Elimination of this side chain at the H95Q mutant results in a dramatic change in the products of wild type TIM-catalyzed isomerization of GAP and of DHAP in tritium-labeled water [19]. It was proposed that this change was due to substitution of the remaining carboxylate side chain of Glu165 for the deleted imidazole of His95 in mediating proton transfer reactions between the enediolate O-1 and O-2, so that this carboxylate effects proton transfer at both carbon and oxygen for the H95Q mutant enzyme-catalyzed reaction. The requirement that the imidazole side chain interact with the O-1 and O-2 oxyanions at the two reaction intermediates (Scheme 1) will limit the strength of the interaction, in order to avoid that interconversion of these intermediates become strongly rate-determining. This provides a simple explanation for the utilization of the weakly basic neutral imidazole side chain [43], instead of the more strongly acidic imidazolium cation.

The cationic side chain of Lys12 runs across the surface of TIM, forms a solvent separated ion pair with the ligand phosphodianion,

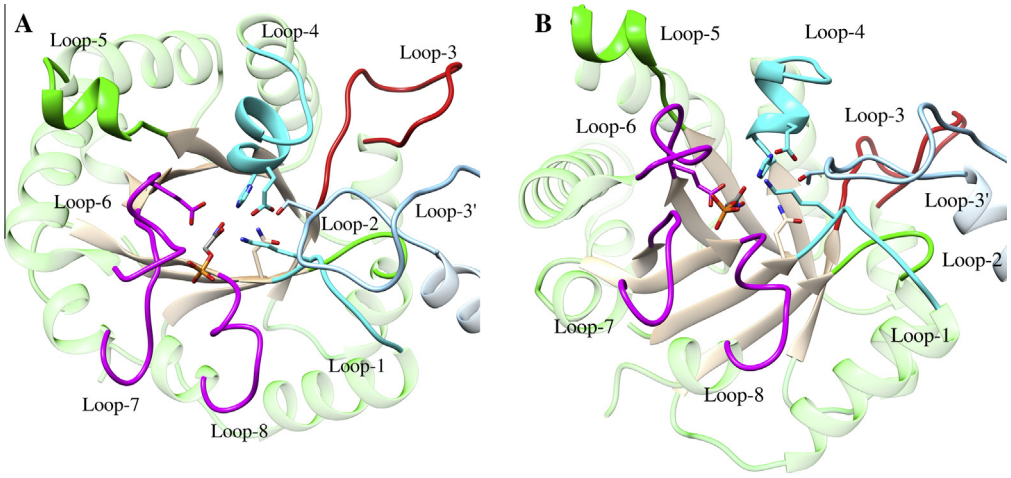

Fig. 1. Cartoons (PDB entry ITPH) drawn to show perspectives of a single subunit of the complex between *c*TIM and the competitive inhibitor phosphoglycolohydroxamate (PGH). The eight βα front loops are labeled, along with loop 3′ provided by the neighboring protein subunit. (A) A view from the "top" of the barrel, which shows the convergence of the catalytic side chains at the active site. The basic side chain from Glu165 (loop 6) abstracts the acidic carbon proton, the acidic side chain from His95 (loop 4) shuttles a proton between the enediolate oxygens, and the acidic side chains of Asn10 and Lys12 (loop 1) stabilize negative charge at these oxygen atoms. (B) A view from the "side" of the barrel, which illustrates the placement of front loops across the "top" of the barrel. The loops are color-coded: loops 1 and 4 are shown in cyan; loop 3 is shown in red; loops 6, 7 and 8 are shown in magenta; loops 2 and 5 are shown in green; and, loop 3′ from the second subunit is shown in light blue.

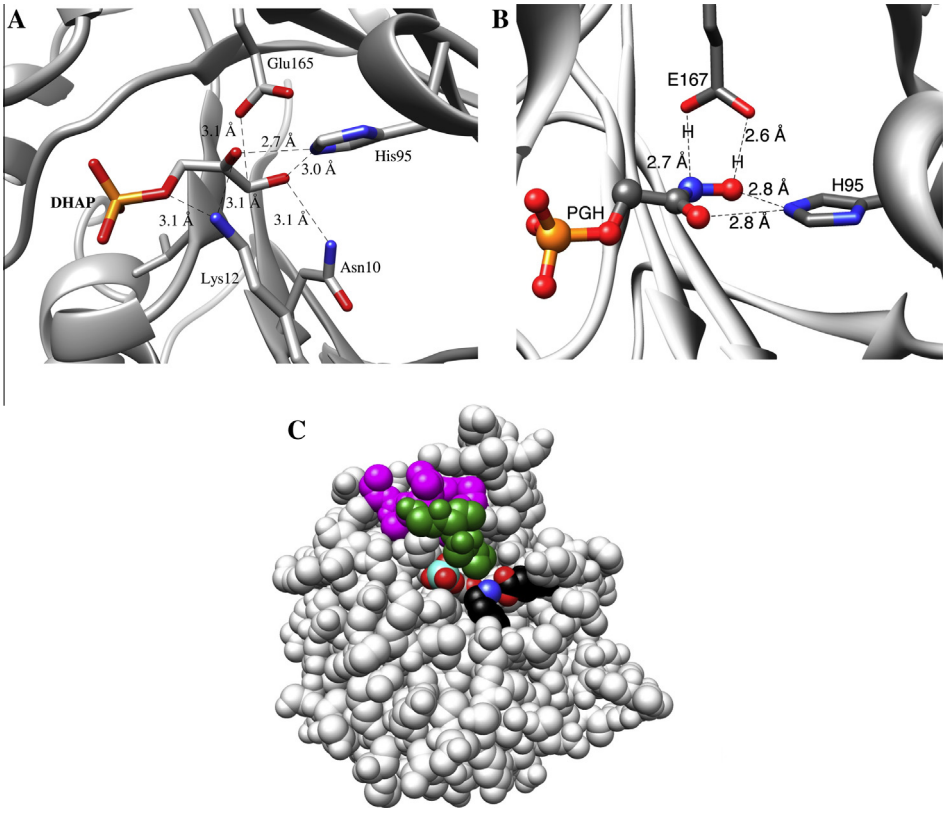

Fig. 2. Representations of X-ray crystal structures of TIM. (A) The active site of yeast TIM complexed to substrate DHAP (PDB entry 1NEY). The acidic side chains ofAsn10, Lys12 and His95 function to stabilize negative charge at the O-1 and O-2 enediolate phosphate intermediates [37]. (B) The complex (0.82 Å resolution) between TIM from *L. mexicana* and the intermediate analog PGH (PDB entry 2VXN), which shows the highly structured interactions between PGH and the side chains of His95 and Glu167 [38].[1] Reprinted with permission from Ref. [20]. (C) A space-filling representation of the surface of yeast TIM (PDB entry 2YPI) in a complex with 2-phosphoglycolate [39]. The residues from the phosphodianion gripper loop six are shaded magenta and green. The green residues were deleted from a loop 6 mutant [40]. The ammonium nitrogen (blue) from the side chain of Lys12 forms as solvent-separated ion pair with the ligand phosphodianion. Reprinted with permission from Ref. [69].

and is part of the cage that locks the ligand into the protein interior (Fig. 2C) [15,20]. An inter loop ion pair between the Lys12 ammonium cation from loop 1 and the Glu97 carboxylate anion from loop 4 [44], presumably promotes effective electrophilic catalysis by Lys12 by holding this side chain in a conformation that provides optimal transition state stabilization [45]. The 6×10^5-fold effect of the K12G mutation on k_{cat}/K_m for catalysis by wild type TIM from yeast corresponds to a 7.8 kcal/mol stabilization of the rate-determining isomerization transition state by the Lys12 side chain cation [41]. About one-third of this effect is due to the ground state interaction between the side-chain cation and the ligand phosphodianion, and the remaining two-thirds is due to the tightening of this interaction at the enediolate trianion-like transition state [41]. This stabilizing interaction is mainly or entirely electrostatic, and is enhanced by the smaller effective local dielectric constant for the active site of TIM, compared with bulk solution [20,46]. The wild type enzyme activity, lost at the K12G mutant TIM, is partly restored by exogenous NH_4^+ and alkylammonium cations [42]. Stabilizing electrostatic interactions between the cation and the transition state trianion, and hydrophobic interactions between the alkyl "arm" and the protein surface both contribute to the efficiency of rescue [42]. The amide side chain of Asn10 is positioned closest to the terminal substrate oxygen, and presumably stabilizes the O-1 enediolate oxyanion. However, the role of Asn10 in catalysis by TIM has not been examined in mutagenesis experiments. These experiments are critical to the development of a complete understanding of the interplay between the side chains of Asn10, Lys12 and His95 (Fig. 2A) during TIM-catalyzed isomerization.

2.2. Loop 3

The active site of TIM is composed entirely of side chains from a single subunit. However, loop 3 (residues 64–79 for *c*TIM) is inserted into a deep crevice, which is located near the active site at the second subunit. In the case of TIM from *Trypanosoma brucei brucei* (*Tbb*TIM) the side chain of Thr75 for subunit A lies 5–6 Å from O-1 of L-glycerol 3-phosphate bound to subunit B [47,48]. The side chain of Thr75 is hydrogen bonded to the Glu97 carboxylate anion from loop 4 of the second subunit, which in turn forms an ion pair with the cationic side chain of Lys13 from loop 1 (Fig. 3A).[1] This network of hydrogen bonds implies a role for loop 3 in maintaining the structure of the TIM active site at the neighboring subunit.

The dimer interface between TIM monomers buries ca. 1600 Å of protein surface [48], and is composed mainly of residues from loops 1–4, with loop 3 residues dominating. In the case of *Tbb*TIM, 203 of 256 non-hydrogen atoms that lie within 4 Å of the subunit interface are from loop 3, and they account for 17 of 20 hydrogen bonding interactions at the interface [49]. Wierenga and coworkers reasoned that intra dimer interactions of loop 3 at the interface play a critical role in stabilizing the dimer, and that reducing these interactions by shortening loop 3 (Scheme 2) would result in a monomeric form of TIM [47]. Their protocol for the design of monomeric TIM focused on the following: (1) the elimination of a hydrophobic patch at loop 3 by deleting central loop residues. (2) Optimizing the conformational stability of the designed protein by including an additional P81A substitution, which allowed for an additional α-turn. This ensured that all of the φψ angles at the

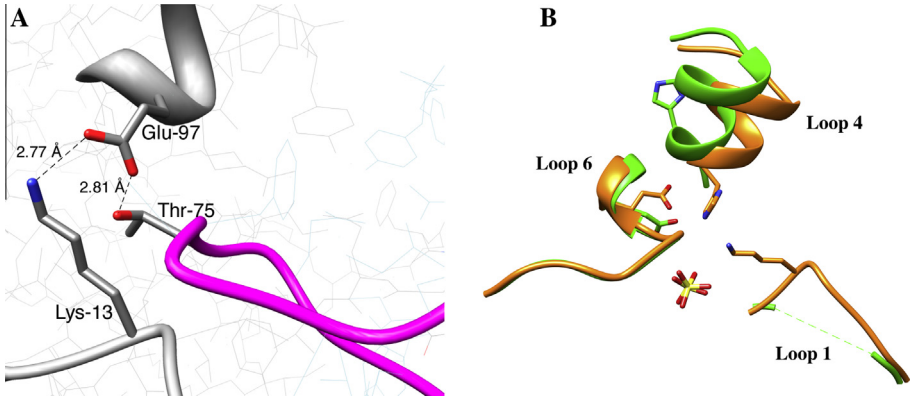

Fig. 3. (A) A representation, from an X-ray crystal structure, which shows the interactions between the Thr75 side chain of loop 3′, and the active site at the neighboring subunit (PDB entry 1TRD). Note the difference in the numbering of the catalytic lysine for yeast TIM (Lys12) and *Tbb*TIM (Lys13).[1] (B) The superposition of crystal structures for wild type *Tbb*TIM (salmon, PDB code 5TIM) and the engineered loop of monoTIM (green, PDB code 1TRI) in a complex with sulfate dianion. The disorder in loop 1, which includes Lys13, leaves a gap in the electron density in the crystal structure for monoTIM. There is a large shift in the position of the imidazole side chain of His95 at monoTIM from that observed for wild type TIM, where the side chain is directed towards the ligand.

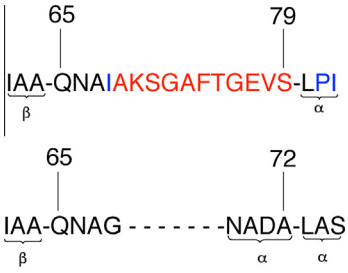

Scheme 2. A comparison of the amino acid sequences for wild type *Tbb*TIM and for the engineered loop of monoTIM: the 15-residue loop 3 of wild type TIM has been replaced by an 8-residue fragment. The additional amino acid substitutions at wild type TIM are shown in blue.

reattached truncated loop lie in the acceptable region of a Ramachandran plot. (3) Reducing the loop hydrophobicity through an I82S mutation [47].

The engineered loop 3 mutation at *Tbb*TIM (Scheme 2) results in a monomeric TIM (monoTIM) with a thermal stability similar to that for wild type TIM, but a reduced catalytic activity, reflective of a 20-fold increase in K_m and a 400-fold decrease in k_{cat} [47,50]. The activity of monoTIM was subsequently improved by directed evolution [51]. X-ray crystal structures of monoTIM show substantial changes in protein structure in the regions of loops 1 and 4 (Fig. 3B) [52–54], consistent with a large increase in the motion of loop 1 and a shift in the position of loop 4. This provides strong evidence that the network of interactions, which extend from loop 3′ from subunit B to loops 4 and then to loop 1 at the active site of wild type TIM (Fig. 3A) contribute to the structural integrity of the enzyme active site.

2.3. Loops 6, 7 and 8

The Michaelis complex of TIM (Fig. 4A) is stabilized by hydrogen bonds between the substrate phosphodianion and backbone amides from loops 6 (residues 165–177 for *c*TIM) and loop 7 (residues 209–216 for *c*TIM) – whose formation is part of a ligand-gated conformational change – and from the rigid loop 8 (residues 232–239 for *c*TIM [39,55]. The flapping of loop 6 is the most prominent element of a change in the conformation of TIM from an open form that is inactive to an active closed form [29,56–58]. This motion is required for substrate binding and product release, which limit the rate of turnover of GAP: [27,59] the barrier to this enzyme conformational change might contribute to the barrier for the binding and release of GAP.

3. Enzyme activation

The flexible structure of TIM enables the conversion of the open form of the free enzyme to a Michaelis complex, where the substrate is "locked" in a catalytic cage [15]. It is self-evident that the open form of TIM shows a low reactivity towards catalysis of isomerization, and that the conformational change transforms TIM to a catalytically active form. The consequences of this enzyme activation were only recently been revealed in studies on the mechanism for phosphite dianion activation of TIM-catalyzed reactions of glycolaldehyde (GA) and [1-^{13}C]-glycolaldehyde ([1-^{13}C]-GA) in D_2O [23,50,60–64].

The binding of phosphite dianion (HP_i) to TIM results in a *ca.* 1000-fold increase in the second-order rate constant for the unactivated isomerization reaction of GA and [1-^{13}C]-GA ([$(k_{cat}/K_m)_E$, Scheme 3A] to $(k_{cat}/K_m)_{E\cdot HPi}$ for catalysis by the enzyme-phosphite complex [23,50,65]. Enzyme activation is rationalized by the model shown in Scheme 3B, where unliganded TIM exists mainly as an inactive open form ($\mathbf{E_O}$), which is in equilibrium with a small amount of the active closed enzyme ($\mathbf{E_C}$, $K_C \approx 1/1000$, Scheme 3B). Phosphite dianion, shows a high affinity for binding to $\mathbf{E_C}$ to form the activated $E_C{\cdot}HP_i$ complex [$(k_{cat}/K_m)_{E'} \approx (k_{cat}/K_m)_{E'\cdot HPi}$, Scheme 3B], with the result that *ca.* 4 kcal/mol of the total dianion binding energy is utilized to drive the conformational equilibrium of TIM from inactive $\mathbf{E_O}$ to active $\mathbf{E_C}{\cdot}HP_i$. [64] Scheme 3B is a general mechanism to avoid the full expression of the ligand binding energy at the Michaelis complex, when this is necessary to avoid tight ligand binding and strongly rate-determining product release [66]. The part of the intrinsic dianion binding energy utilized to drive the enzyme conformational change will not be expressed at the Michaelis complex (K_m effect), but rather will result in a high enzyme reactivity toward deprotonation of bound carbon acid substrate (k_{cat} effect) [6].

The essential features of Scheme 3B are: (1) the large thermodynamic barrier for conversion of TIM from the inactive open to the active closed form. (2) The active role of HP_i in providing the "glue" to hold the enzyme in the closed form. (3) The spectator role of HP_i, which does not directly interact with the transition state for TIM-catalyzed proton transfer reaction, or affect the structure of this transition state. The model shown in Scheme 3B is strongly supported by the observation that a large number of site-directed

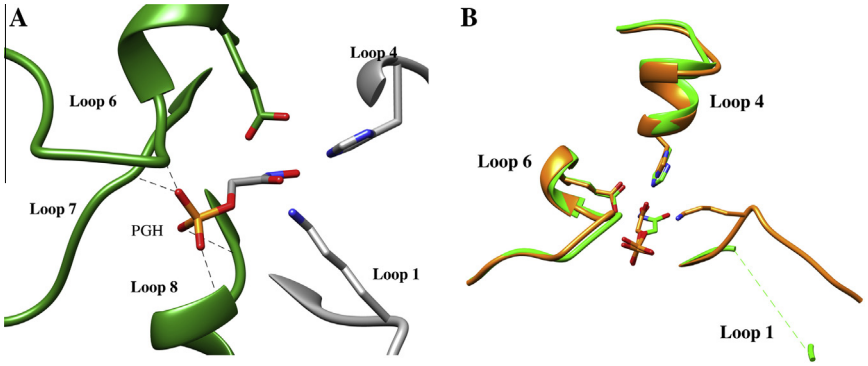

Fig. 4. (A) A representation, from an X-ray crystal structure, which shows the organization of loops 6, 7 and 8 around the phosphodianion of the PGH ligand. The dashed lines show the hydrogen bonds between backbone amides from loops 6 (one H-bond) and 7 (one H-bond), and loop 8 (two H-bonds) and the ligand phosphodianion. (B) Superimposed X-ray crystal structures, of wild type *Tbb* TIM (orange, PDB code 5TRD) and the engineered monoTIM (green, PDB code 1TTJ) in a complex with PGH. The binding of PGH to monoTIM results in a large shift in the position of loop 4 (see Fig. 3B), which is now congruent with loop 4 from wild type TIM. Loop 1 of monoTIM remains disordered in the PGH complex.

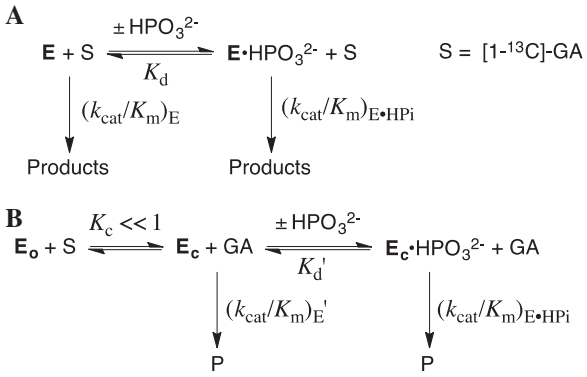

Scheme 3. Schemes used to model kinetic data for TIM-catalyzed reactions of GA and [1-^{13}C]-GA.

mutations of TIM result in the same change in the activation barrier to the reaction of the whole substrate GAP and of the substrate pieces [1-^{13}C]-GA + HP_i [60]. This result supports the spectator role of HP_i, by showing that the transition states for the reactions of the *whole substrate* and the *substrate pieces* are stabilized by similar interactions with the protein catalyst, so that by this criteria the transition states have the same structure [60].

There is good evidence that the barrier to loop closure, in isolation from the other elements of the enzyme conformational change, is not large [32,33,36]. We have proposed that the *ca* 4 kcal/mol barrier to K_C required to rationalize enzyme activation by HP_i results partly or entirely from the barrier to extrusion of solvent water from the enzyme active site [6,15,20,67]. Enzyme activation by the conformational change of TIM has been linked to: (a) the development of a steric clash between the carbonyl oxygen of Gly209 and the pyrolidine ring of Pro166 [56], which is relieved by movement of this side chain that carries the side chain of Glu165 by 2 Å towards the carbon acid substrate. (b) The desolvation of the carboxylate side chain from Glu165 [15,67]. (c) The placement of the basic Glu167 side chain in a hydrophobic clamp created by the side chains of Ile172 and Leu232 [58,62,63]. This clamp results in $a > 2$ unit higher pK_a for the carboxylic acid side chain of Glu167 at wild type *Tbb*TIM compared with the I172A mutant enzyme [68].[1]

4. Structural mutants of TIM

Mutations, which distort the structure of unliganded TIM ($\mathbf{E_O}$, Scheme 3B) result in an increase in the barrier to the enzyme conformational change (decrease in K_C), an increase in the substrate binding energy utilized to drive the change from $\mathbf{E_O}$ to $\mathbf{E_C}$, and a decrease in the second order rate constant k_{cat}/K_m for TIM-catalyzed isomerization. There is good evidence that the effects of these mutations may be overcome by the utilization of substrate binding energy to restore the structure of the mutant TIMs to the active closed form.

(1) The loop 3 mutation, which was engineered to stabilize monomeric TIM relative to the dimer, results in disorder for the side chain of Lys13 and a large shift in the imidazole side chain of His95 at the unliganded enzyme (Fig. 3B). However, the K13A and H95A mutations of monoTIM each result in a falloff in catalytic activity: this shows that these amino acid side chains interact with the transition state for the monoTIM-catalyzed isomerization reaction. The binding of the intermediate analog PGH to monoTIM results in a global conformational change, which includes motion of loops 6 and 7 and *additional movement of loop 4* that positions the catalytic side chains of His95 to interact with the transition state for enzyme-catalyzed isomerization (Fig. 4B). The lower catalytic activity of monoTIM compared to the wild type enzyme is therefore partly due to the requirement that additional ligand binding energy be utilized to drive a conformational change of loop 4, which leaves a smaller fraction of the substrate binding energy available to stabilize the isomerization reaction transition state [6,66].

(2) A loop 6 replacement mutant (L6RM) of *c*TIM, where the eukaryotic N-terminal hinge sequence, 166-PXW-168 [X = L, V], is replaced by the sequence from archaebacteria, 166-PPE-168 has been examined [69]. A comparison of the X-ray crystal structures for wild type *c*TIM (Fig. 5A and B) and the L6RM (Fig. 5B) shows that the mutation introduces a kink into loop 6 and a displacement of the side chain of Glu168 from the position of the tryptophan side chain of Trp168 for wild type TIM. This kink presumably reduces the destabilizing interactions between the carboxylate side chain of Glu168 and Glu129 (Fig. 5A and B). Closure of loop 6 at archaeal TIM is enabled by the replacement of Trp168 at the functionally equivalent position in the protein, by Glu147, which forms a salt bridge with the side chain of Lys159 (Fig. 5C) [70–72].

The L6RM mutant shows a reduced activity compared to wild type TIM. The transition state for the L6RM-catalyzed isomerization is stabilized by interactions with loop 6, since the activity of

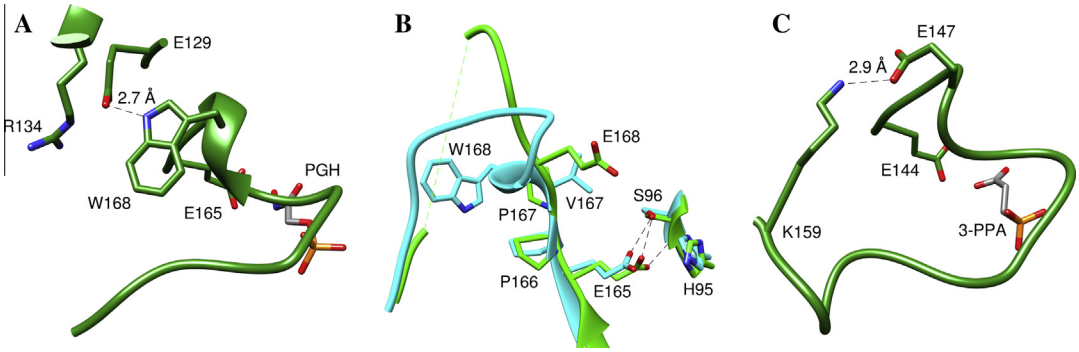

Fig. 5. Representations from X-ray crystal structures of TIM at the N-terminal hinge of loop 6. (A) The complex between PGH and wild type *c*TIM, which shows the hydrogen bond between the Glu129 and Trp168 side chains (PDB entry 1TPH). (B) Superimposed X-ray crystal structures of unliganded wild type *c*TIM (blue ribbon, PDB entry 1TIM) and the unliganded L6RM of *c*TIM (green ribbon, PDB entry 4P61). Note the displacement of the side chain for Glu168, presumably to avoid interactions with the Glu129 side chain. The L6RM, has no significant electron density from residues 173–175 of loop 6. (C) TIM from *Pyrococcus woesei* liganded to 3-phosphonopropanoic acid (PDB entry 1HG3). The carboxylate side chain of the hinge residue Glu147, which occupies a position equivalent to that of Trp168 from wild type *c*TIM and Glu168 for the L6RM of *c*TIM, is stabilized by a hydrogen bond to the cationic side chain of Lys159. Reprinted with permission from Ref. [69].

the L6RM is substantially higher than for a loop 6 deletion mutant (LDM) [40,69]. The absence of a functioning loop at the LDM results in a change in the preferred catalyzed reaction from aldose-ketose isomerization to elimination of inorganic phosphate trianion to form methylgloxal [40,73] *No elimination reaction products are observed for the L6RM* [69]. This shows that the L6RM-catalyzed reaction is through a catalytically active closed enzyme ($\mathbf{E_C}$, Scheme 3B), which is stabilized towards elimination of PO_4^{3-} by interactions between loop 6 and the enediolate phosphate intermediate.

The failure to *detect* binding by 10 mM GAP and DHAP, or by 10 mM of the intermediate analog 2-phosphoglycolate (PGA) shows that essentially all of the ligand binding energy for the L6RM is utilized to drive a change in conformation from $\mathbf{E_O}$ to a closed enzyme $\mathbf{E_C}$ (Scheme 3B) that is destabilized by an electrostatic interaction between the carboxylate side chains of Glu168 and Glu129 (Fig. 5A and B); and, that little or no binding energy remains to stabilize the Michaelis complex [69] These results provide a remarkable example of the *plasticity* of the structure of this TIM barrel [74], where the severe distortion in structure of the unliganded wild type enzyme (Fig. 5B) at the L6RM is overcome by the utilization of substrate binding energy to mold the enzyme into the active closed form.

5. Origin of the catalytic power of the TIM-barrel

We now consider the properties of the TIM-barrel architecture, which favor its propagation as a catalyst of a multitude of chemical reactions.

(1) The repeating α- and β-secondary structural elements of the TIM-barrel provide a constant fixed scaffold onto which many different enzyme active sites may be constructed.
(2) Mutations of protein structure generally decrease protein stability, so that mutations that enhance function will often require compensating mutations that enhance protein stability [75,76]. The separation of the front loops at the "catalytic" end of the TIM-barrel and the back loops at the "stability" end (Fig. 1B) is well adapted for rapid evolution. This architecture allows function-enhancing mutations at the "catalytic" end of the barrel to be compensated for by mutations at the stability end.
(3) Protein folds which incorporate catalytic side chains into the secondary structural scaffold, such as the ⩾60% of the side chains found at the scaffold for dihydrofolate reductase, tend to support only a single function during the course of evolution [77]. This is probably a consequence of the rigidity of α-helical and β-sheet secondary elements, which restrict the number of intra and inter subunit conformations for their amino acid side chains. By contrast, about 80% of the active site side chains of the TIM-barrels are part of flexible loops [77]. These loops show a far larger range of conformational states, which provide for a greater range of active site structures.
(4) The diversity provided by the eight front loops of the TIM-barrel allows for the construction of enzyme active sites that show a range of broad range of functions.
(5) There is increasing evidence that the catalytically active form of enzymes, which utilize phosphodianion gripper loops [6,64,78–81], is present as only a small fraction of the total protein, and that the dianion binding energy is utilized to drive an activating change in protein conformation [6]. The highly flexible, *plastic*, protein loops allow for the utilization of dianion binding energy to mold TIM barrels into a catalytically active closed form.

Acknowledgment

The work from the author's laboratory, described in this review, was supported by Grant GM 39754 from the National Institutes of Health.

References

[1] J.P. Richard, Biochemistry 52 (2013) 2009–2011.
[2] J.P. Klinman, Biochemistry 52 (2013) 2068–2077.
[3] D. Herschlag, A. Natarajan, Biochemistry 52 (2013) 2050–2067.
[4] Y. Fan, A. Cembran, S. Ma, J. Gao, Biochemistry 52 (2013) 2036–2049.
[5] S. Hammes-Schiffer, Biochemistry 52 (2012) 2012–2020.
[6] T.L. Amyes, J.P. Richard, Biochemistry 52 (2013) 2021–2035.
[7] J.A. Gerlt, P.C. Babbitt, Nat. Struct. Biol. 8 (2001) 5–7.
[8] R.K. Wierenga, FEBS Lett. 492 (2001) 193–198.
[9] R. Sterner, B. Hocker, Chem. Rev. 105 (2005) 4038–4055.
[10] N. Nagano, C.A. Orengo, J.M. Thornton, J. Mol. Biol. 321 (2002) 741–765.
[11] B. Höcker, C. Jürgens, M. Wilmanns, R. Sterner, Curr. Opin. Biotechnol. 12 (2001) 376–381.
[12] J.A. Gerlt, F.M. Raushel, Curr. Opin. Chem. Biol. 7 (2003) 252–264.
[13] J.A. Gerlt, P.C. Babbitt, Annu. Rev. Biochem. 70 (2001) 209–246.
[14] E. Wise, W.S. Yew, P.C. Babbitt, J.A. Gerlt, I. Rayment, Biochemistry 41 (2002) 3861–3869.
[15] J.P. Richard, T.L. Amyes, B. Goryanova, X. Zhai, Curr. Opin. Chem. Biol. 21 (2014) 1–10.
[16] F.C. Hartman, H. Ratrie III, Biochem. Biophys. Res. Commun. 77 (1977) 746–752.
[17] S. De la Mare, A.F.W. Coulson, J.R. Knowles, J.D. Priddle, R.E. Offord, Biochem. J. 129 (1972) 321–331.

[18] E.A. Komives, L.C. Chang, E. Lolis, R.F. Tilton, G.A. Petsko, J.R. Knowles, Biochemistry 30 (1991) 3011–3019.
[19] E.B. Nickbarg, R.C. Davenport, G.A. Petsko, J.R. Knowles, Biochemistry 27 (1988) 5948–5960.
[20] J.P. Richard, Biochemistry 51 (2012) 2652–2661.
[21] I. Kursula, S. Partanen, A.-M. Lambeir, D.M. Antonov, K. Augustyns, R.K. Wierenga, Eur. J. Biochem. 268 (2001) 5189–5196.
[22] P.J. Lodi, L.C. Chang, J.R. Knowles, E.A. Komives, Biochemistry 33 (1994) 2809–2814.
[23] M.K. Go, T.L. Amyes, J.P. Richard, Biochemistry 48 (2009) 5769–5778.
[24] A.C. O'Donoghue, T.L. Amyes, J.P. Richard, Org. Biomol. Chem. 6 (2008) 391–396.
[25] A.C. O'Donoghue, T.L. Amyes, J.P. Richard, Biochemistry 44 (2005) 2622–2631.
[26] A.C. O'Donoghue, T.L. Amyes, J.P. Richard, Biochemistry 44 (2005) 2610–2621.
[27] J.R. Knowles, W.J. Albery, Acc. Chem. Res. 10 (1977) 105–111.
[28] X. Zhai, M.M. Malabanan, T.L. Amyes, J.P. Richard, J. Phys. Org. Chem. 27 (2014) 269–276.
[29] R.K. Wierenga, Cell. Mol. Life Sci. 67 (2010) 3961–3982.
[30] J.R. Knowles, Nature 350 (1991) 121–124.
[31] J.R. Knowles, Philos. Trans. R. Soc. London, Ser. B 332 (1991) 115–121.
[32] S. Rozovsky, A.E. McDermott, J. Mol. Biol. 310 (2001) 259–270.
[33] S. Rozovsky, G. Jogl, L. Tong, A.E. McDermott, J. Mol. Biol. 310 (2001) 271–280.
[34] J.P. Loria, R.B. Berlow, E.D. Watt, Acc. Chem. Res. 41 (2008) 214–221.
[35] J.G. Kempf, J.-Y. Jung, C. Ragain, N.S. Sampson, J.P. Loria, J. Mol. Biol. 368 (2007) 131–149.
[36] R. Desamero, S. Rozovsky, N. Zhadin, A. McDermott, R. Callender, Biochemistry 42 (2003) 2941–2951.
[37] G. Jogl, S. Rozovsky, A.E. McDermott, L. Tong, Proc. Natl. Acad. Sci. 100 (2003) 50–55.
[38] M. Alahuhta, R.K. Wierenga, Prot.: Struct., Funct. Bioinf. 78 (2010) 1878–1888.
[39] E. Lolis, G.A. Petsko, Biochemistry 29 (1990) 6619–6625.
[40] D.L. Pompliano, A. Peyman, J.R. Knowles, Biochemistry 29 (1990) 3186–3194.
[41] M.K. Go, A. Koudelka, T.L. Amyes, J.P. Richard, Biochemistry 49 (2010) 5377–5389.
[42] M.K. Go, T.L. Amyes, J.P. Richard, J. Am. Chem. Soc. 132 (2010) 13525–13532.
[43] P.J. Lodi, J.R. Knowles, Biochemistry 30 (1991) 6948–6956.
[44] M. Samanta, M.R.N. Murthy, H. Balaram, P. Balaram, Chembiochem 12 (2011) 1886–1895.
[45] A. Warshel, J. Biol. Chem. 273 (1998) 27035–27038.
[46] J. Hine, Structural Effects on Equilibria in Organic Chemistry, John Wiley & Sons, New York, 1975.
[47] T.V. Borchert, R. Abagyan, R. Jaenicke, R.K. Wierenga, Proc. Natl. Acad. Sci. 91 (1994) 1515–1518.
[48] R.K. Wierenga, M.E.M. Noble, G. Vriend, S. Nauche, W.G.J. Hol, J. Mol. Biol. 220 (1991) 995–1015.
[49] R.K. Wierenga, M.E.M. Noble, R.C. Davenport, J. Mol. Biol. 224 (1992) 1115–1126.
[50] M.M. Malabanan, M. Go, T.L. Amyes, J.P. Richard, Biochemistry 50 (2011). 5679–5767.
[51] G. Saab-Rincón, V.R. Juárez, J. Osuna, F. Sánchez, X. Soberón, Prot. Eng. 14 (2001) 149–155.
[52] W. Schliebs, N. Thani, R. Eritja, R. Wierenga, Prot. Sci. 5 (1996) 229–239.
[53] T.V. Borchert, K.V.R. Kishan, J.P. Zeelen, W. Schliebs, N. Thanki, R. Abagyan, R. Jaenicke, R.K. Wierenga, Structure 3 (1995) 669–679.
[54] T.V. Borchert, R. Abagyan, K.V.R. Kishan, J.P. Zeelen, R.K. Wierenga, Structure 1 (1993) 205–213.
[55] R.C. Davenport, P.A. Bash, B.A. Seaton, M. Karplus, G.A. Petsko, D. Ringe, Biochemistry 30 (1991) 5821–5826.
[56] M.G. Casteleijn, M. Alahuhta, K. Groebel, I. El-Sayed, K. Augustyns, A.M. Lambeir, P. Neubauer, R.K. Wierenga, Biochemistry 45 (2006) 15483–15494.
[57] I. Kursula, M. Salin, J. Sun, B.V. Norledge, A.M. Haapalainen, N.S. Sampson, R.K. Wierenga, Prot. Eng., Des. Sel. 17 (2004) 375–382.
[58] I. Kursula, R.K. Wierenga, J. Biol. Chem. 278 (2003) 9544–9551.
[59] W.J. Albery, J.R. Knowles, Biochemistry 15 (1976) 5627–5631.
[60] X. Zhai, T.L. Amyes, J.P. Richard, J. Am. Chem. Soc. 136 (2014) 4145–4148.
[61] X. Zhai, T.L. Amyes, R.K. Wierenga, J.P. Loria, J.P. Richard, Biochemistry 52 (2013) 5928–5940.
[62] M.M. Malabanan, A.P. Koudelka, T.L. Amyes, J.P. Richard, J. Am. Chem. Soc. 134 (2012) 10286–10298.
[63] M.M. Malabanan, T.L. Amyes, J.P. Richard, J. Am. Chem. Soc. 133 (2011) 16428–16431.
[64] T.L. Amyes, J.P. Richard, Biochemistry 46 (2007) 5841–5854.
[65] T.L. Amyes, J.P. Richard, Proton Transfer to and from carbon in model systems, in: J.T. Hynes, J.P. Klinman, H.-H. Limbach, R.L. Schowen (Eds.), Hydrogen-Transfer Reactions, Volume 3, Biological Aspects I–II, Wiley-VCH, Weinheim, 2007, pp. 949–973.
[66] W.P. Jencks, Adv. Enzymology Relat. Areas Mol. Biol. 43 (1975) 219–410.
[67] M.M. Malabanan, T.L. Amyes, J.P. Richard, Curr. Opin. Struct. Biol. 20 (2010) 702–710.
[68] M.M. Malabanan, L. Nitsch-Velasquez, T.L. Amyes, J.P. Richard, J. Am. Chem. Soc. 135 (2013) 5978–5981.
[69] X. Zhai, M.K. Go, A.C. O'Donoghue, T.L. Amyes, S.D. Pegan, Y. Wang, J.P. Loria, A.D. Mesecar, J.P. Richard, Biochemistry 53 (2014) 3486–3501.
[70] P. Gayathri, M. Banerjee, A. Vijayalakshmi, S. Azeez, H. Balaram, P. Balaram, M.R.N. Murthy, Acta Crystallogr. D Biol. Crystallogr. 63 (2007) 206–220.
[71] H. Walden, G. Taylor, H. Lilie, T. Knura, R. Hensel, Biochem. Soc. Trans. 32 (2004) 305.
[72] H. Walden, G.S. Bell, R.J. Russell, B. Siebers, R. Hensel, G.L. Taylor, J. Mol. Biol. 306 (2001) 745–757.
[73] J.P. Richard, J. Am. Chem. Soc. 106 (1984) 4926–4936.
[74] A.E. Todd, C.A. Orengo, J.M. Thornton, Trends Biochem. Sci. 27 (2002) 419–426.
[75] J.D. Bloom, S.T. Labthavikul, C.R. Otey, F.H. Arnold, Proc. Natl. Acad. Sci. 103 (2006) 5869–5874.
[76] N. Tokuriki, D.S. Tawfik, Science 324 (2009) 203–207.
[77] E. Dellus-Gur, A. Toth-Petroczy, M. Elias, D.S. Tawfik, J. Mol. Biol. 425 (2013) 2609–2621.
[78] B. Goryanova, T.L. Amyes, J.A. Gerlt, J.P. Richard, J. Am. Chem. Soc. 133 (2011) 6545–6548.
[79] W.-Y. Tsang, T.L. Amyes, J.P. Richard, Biochemistry 47 (2008) 4575–4582.
[80] T.L. Amyes, J.P. Richard, J.J. Tait, J. Am. Chem. Soc. 127 (2005) 15708–15709.
[81] W.J. Ray Jr., J.W. Long, J.D. Owens, Biochemistry 15 (1976) 4006–4017.